frontiers in Physics

REVIEW
published: 07 May 2021
doi: 10.3389/fphy.2021.654374

Acoustically-Stimulated Nanobubbles: Opportunities in Medical Ultrasound Imaging and Therapy

Brandon Helfield[1,2], *Yiran Zou*[3] *and Naomi Matsuura*[3,4,5]*

[1] *Department of Physics, Concordia University, Montreal, QC, Canada,* [2] *Department of Biology, Concordia University, Montreal, QC, Canada,* [3] *Department of Materials Science and Engineering, University of Toronto, Toronto, ON, Canada,* [4] *Insititute of Biomedical Engineering, University of Toronto, Toronto, ON, Canada,* [5] *Department of Medical Imaging, University of Toronto, Toronto, ON, Canada*

Medical ultrasound is one of the most widely used imaging modalities worldwide. Microbubbles, typically ∼1–8 μm in diameter, are ultrasound contrast agents confined to the vasculature due to their size. Microbubbles have broadened the scope of medical ultrasound, permitting real-time imaging of the microvasculature for blood flow assessment, molecular imaging, and even non-invasive site-specific therapy. Recently, there has been increasing interest in developing submicron, "nanoscale" agents to extend the utility of medical ultrasound. In this review, we discuss the development of lipid-encapsulated, acoustically responsive, nanobubbles (∼200–800 nm in diameter), a next-generation ultrasound contrast agent. First, medical ultrasound and bubble-based contrast agents are introduced, followed by the advantages of scaling down bubble size from an acoustic and biological viewpoint. Next, we present how lipid-encapsulated nanobubbles can be developed toward meeting clinically meaningful endpoints, from agent synthesis and characterization to *in vivo* considerations. Finally, future opportunities of nanobubbles for advanced applications in ultrasound diagnostic and therapeutic medicine are proposed.

Keywords: nanobubble, ultrasound imaging and therapy, ultrasound contrast agent, focused ultrasound, submicron bubble, bubble cavitation, non-linear dyanamics, scattering

OPEN ACCESS

Edited by:
Nikolai F. Bunkin, Bauman Moscow State Technical University, Russia

Reviewed by:
Agata A. Exner, Case Western Reserve University, United States
Firouzeh Sabri, University of Memphis, United States

***Correspondence:**
Naomi Matsuura
naomi.matsuura@utoronto.ca

Specialty section:
This article was submitted to Interdisciplinary Physics, a section of the journal Frontiers in Physics

Received: *16 January 2021*
Accepted: *06 April 2021*
Published: *07 May 2021*

Citation:
Helfield B, Zou Y and Matsuura N (2021) Acoustically-Stimulated Nanobubbles: Opportunities in Medical Ultrasound Imaging and Therapy. Front. Phys. 9:654374. doi: 10.3389/fphy.2021.654374

OVERVIEW OF BIOMEDICAL ULTRASOUND AND BUBBLE-BASED CONTRAST AGENTS

Medical imaging, the process of non-invasively "seeing" inside a patient to diagnose disease, is a foundation of modern clinical medicine. One of the most common imaging modalities for the assessment of soft tissue and large vessel blood flow is medical ultrasound [1]. In contrast to x-ray-based imaging (computed tomography, mammography and planar x-ray imaging) and nuclear imaging (positron emission tomography, or single photon emission computed tomography), ultrasound uses mechanical waves as opposed to ionizing radiation and is thus safe for high-risk patients including pregnant women and infants. Unlike magnetic resonance imaging, medical ultrasound permits real-time imaging with small footprint, user-friendly, and are relatively inexpensive systems. These factors make ultrasound one of the most widely used and versatile imaging modalities worldwide [1].

An ultrasound pulse, generally between 1 and 10 MHz and a few cycles in duration, is transmitted from the ultrasound probe into the body. The ultrasound waves are reflected and backscattered at interfaces between tissues with different acoustic impedances (i.e., materials with different densities and sound wave speeds) which are then received by the same probe. In the conventional focused "pulse-echo" approach, the reflected wave transit times and intensities are processed line by line to form an image, typically a 2D cross-section of the body. The frame rate is determined by the sum of the time it takes to transmit a beam and to receive and process the scattered emissions for every line in the image. This is typically ∼10–100 Hz depending on the imaging depth [1]. Image resolution is fundamentally dictated by the transmit frequency f (e.g., wavelength λ) and pulse duration. The lateral and axial resolution are $R_L \propto \lambda f_\#$ and $R_A \propto \lambda f_\#^2$, respectively, where $f_\#$ (often referred to as the f-number) is the ratio of the focal length to the transducer aperture diameter. As ultrasound waves propagate within the body, energy is lost due to absorption and scattering, and the wave is attenuated. To a good approximation, the frequency dependence of attenuation in soft tissue is $\alpha(f) = \alpha_0 f^n$, with $1 \leq n \leq 2$, and typical attenuation coefficients (α_0) range from ∼0.3–0.6 dB/cm/MHz [2]. This represents a fundamental trade-off in ultrasound imaging between spatial resolution and imaging depth, whereby lower frequencies (1–6 MHz) are used to assess deeper tissues (e.g., kidney [3], heart [4]) while higher frequencies (∼7–10 MHz) are used to assess superficial tissues (e.g., carotid artery [5], breast [6]).

The scattering from blood, however, is at least two orders of magnitude weaker than that of tissue [2]. For larger vessels that are millimeters to centimeters in diameter, the relative motion of the red blood cells compared to the surrounding tissue can be exploited to assess blood flow characteristics via pulse-wave Doppler techniques [1]. A fundamental limitation of ultrasound imaging is its inability to image the microvasculature, where these Doppler approaches are hindered by tissue motion, slow blood velocity, and low hematocrit percentage. Indeed, there is a clinical need to image the microvasculature, as it plays a key role in the propagation and treatment of many diseases, including cancer [7], cardiovascular diseases [8], and infectious disease [9]. An improved understanding of the microvasculature can allow clinicians to deliver improved therapies tailored to the characteristics of the individual patient's disease.

Thus, to allow for selective ultrasound imaging of the blood pool, microbubble ultrasound contrast agents are used. In general, contrast agents are exogenous, engineered materials that are designed to differentially scatter, absorb, or emit energy compared to surrounding tissues and inherent background noise. Ultrasound contrast agents remain intravascular post-injection: they consist of a solution of high-density, fluorocarbon gas-filled (e.g., C_4F_{10}, C_3F_8, SF_6), lipid, protein or polymer shell-stabilized microbubbles between 1-8 μm in diameter (10^9-10^{10} microbubbles/mL) [10, 11] (**Figure 1A**). Owing to the high compressibility of the gas core and its flexible shell, microbubbles radially oscillate in an ultrasound field and possess scattering cross-sections on the order of 1,000 times their geometric cross-sections [12]. Given their size and material properties (e.g., shell stiffness and viscosity), microbubbles display resonance characteristics within the diagnostic range of ultrasound imaging (1–10 MHz). Since microbubbles elicit highly non-linear vibration behaviours (e.g., harmonic components) not exhibited by tissue, microbubble echoes in small vessels can be separated from those of the surrounding tissues using specific pulse sequences [13, 14] to generate a bubble-specific image. This emphasizes signal from the vasculature while suppressing non-bubble (tissue) signals, resulting in the ability to specifically image the blood pool with high signal-to-noise and contrast-to-noise ratios. Another unique feature of microbubbles is that they can be made to disrupt, or "pop," under moderate transmit amplitude conditions. This technique, termed disruption-replenishment, results in a local "void" of microbubbles in the blood vessels which then re-fills at a rate that is dependent on blood flow characteristics [15, 16]. This dynamic, real-time imaging of the blood flow allows clinicians to distinguish between abnormal filling patterns characteristic of disease, and their healthy tissue counterparts. As such, ultrasound contrast imaging is routinely employed clinically in echocardiography applications [17], with increasing use in diagnosing diseases in the abdomen (e.g., liver, kidney, pancreas, and spleen) [18].

In addition to microvascular flow imaging, contrast enhanced ultrasound is being evaluated for molecular imaging of the vasculature. Here, microbubbles with targeting ligands attached to their shells actively bind to molecular expressions of disease states, specifically endothelial markers associated with diseases such as cancer or atherosclerosis [10, 19]. Using specific pulsing schemes, contrast images formed from bound, molecularly targeted microbubbles may be used as an indicator of disease progression (**Figure 1B**). Microbubble agent BR55 with targeting specificity for vascular endothelial growth factor receptor (VEGFR2) is currently in clinical trials for the assessment of prostate cancer (NCT02142608), ovarian cancer (NCT03493464) and pancreatic lesions (NCT03486327).

Beyond imaging, microbubbles have found tremendous application in targeted and image-guided therapeutics. Under specific acoustic conditions, microbubbles can elicit local and reversible increases in the permeability of cell membranes and the vasculature, generally termed sonoporation [20, 21]. Through co-injection of a therapeutic or the attachment of therapeutic cargo to the microbubble itself, ultrasound-triggered microbubbles have shown promise for targeted treatment of various cancers and cardiovascular diseases (**Figure 1C**) [22, 23]. Current clinical trials using this technology are ongoing, for example, in the treatment of glioblastoma [24] and Alzheimer's disease [25].

Indeed, one of the strengths of microbubbles as a contrast agent is that they remain intravascular due to their size, allowing for diagnostic measurements that would be otherwise difficult with diffusible tracers. However, there is a growing focus on extending the utility of bubble-based ultrasound approaches toward the extravascular compartment by developing submicron, "nanoscale" ultrasound contrast agents. Numerous medicinal solid and liquid-based nanoscale agents have been developed over many decades, primarily to take advantage of their size-based *in vivo* biological behaviour [26]. For example, nanoscale agents can passively accumulate in tissue by extravasating from the blood

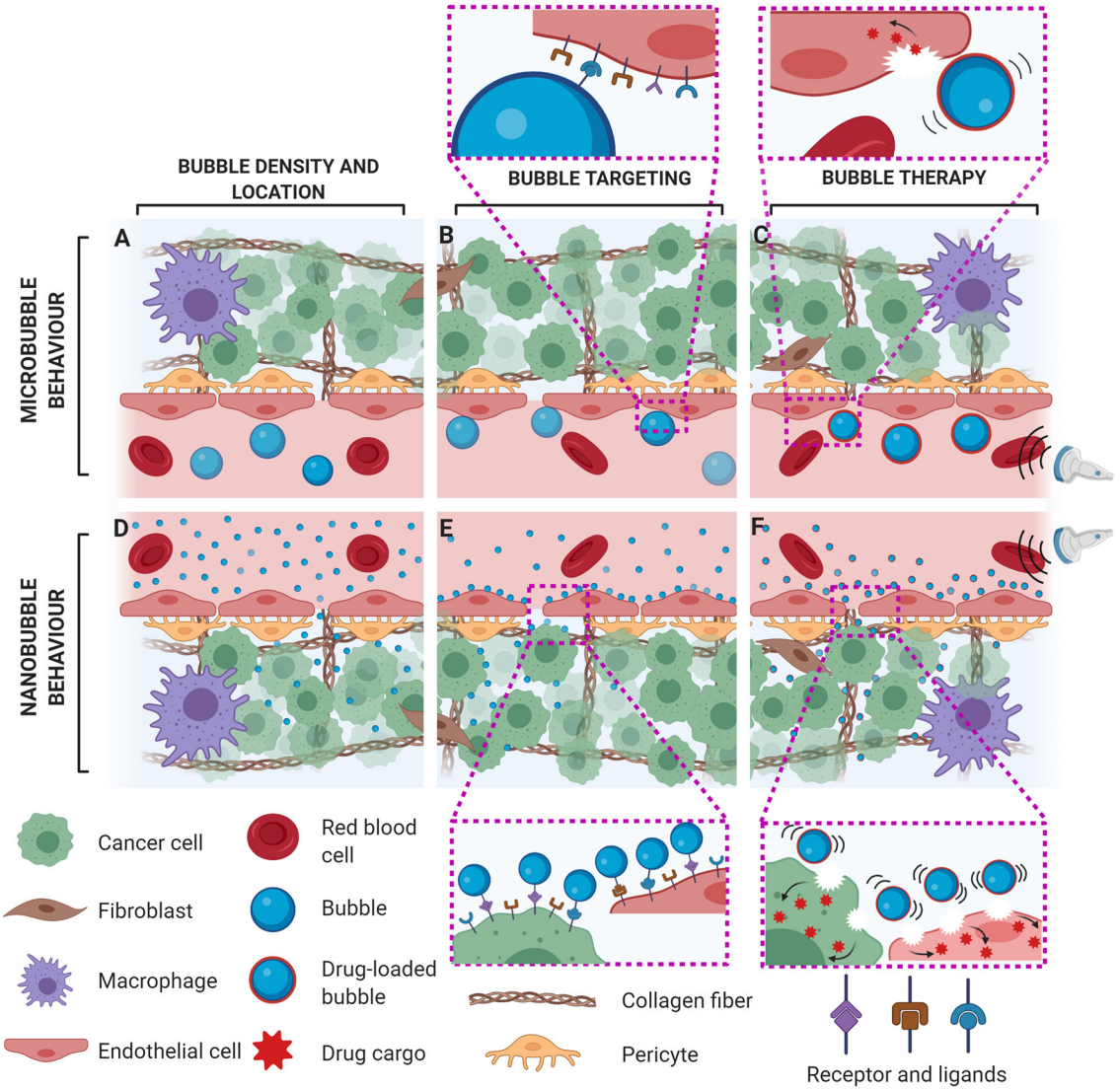

FIGURE 1 | Potential impact of bubble size on acoustic and biological behaviour with microbubbles **(A–C)** and nanobubbles **(D–F)** in leaky vasculature (e.g., in tumours). For the same gas volume, intravascular microbubbles are present in fewer number **(A)** in comparison to nanobubbles, which may also preferentially leak out of pathological neovessels into the tumour interstitium **(D)**. While microbubble-based molecular imaging is limited to vascular targets **(B)**, nanobubbles can bind to both intra- and extravascular biomarkers, in addition to providing a more direct correlation between bubble echo and molecular density **(E)**. Ultrasound-facilitated bubble cavitation of drug-loaded bubbles can induce sonoporation to permeabilize the cell membrane for enhanced transcellular transport of their released therapeutic cargo. In comparison to microbubbles which can only directly perforate endothelial cells **(C)**, nanobubbles can permeabilize both endothelial and cancer cells, leading to enhanced therapeutic efficacy **(F)**.

stream across pathological endothelial fenestrations, typically on the order of 100–800 nm [27] or can be targeted to specific extravascular biological cellular targets to prevent efflux of this agent back to the bloodstream [28]. In the field of ultrasound imaging and therapy, this is an exciting prospect that can unlock the potential of extravascular-specific imaging, bubble-specific association with extravascular targeted moieties, and enhanced ultrasound-mediated therapeutics.

Submicron ultrasound contrast agents currently under investigation include nanobubbles [29, 30], phase-shift nanodroplets [31–33], gas vesicles [34, 35], echogenic liposomes [36] and polymeric nanoparticles [37]. In this review, we will focus on acoustically responsive nanobubbles, a term generally used to describe gas-filled bubbles in the submicron size range, typically on the order of several hundreds of nanometers in size, which are stabilized with a pliable, lipid-based shell (e.g., DPPC, DPSC, DSPC, DPPA and a PEGylated emulsifier) [11, 38]. In contrast to microbubbles that are typically confined to the vasculature, nanobubbles may have the potential to extravasate into interstitial spaces through defective endothelial junctions (**Figure 1D**), and therefore have been proposed for extravascular tumour imaging [29]. Moreover, compared to more sparsely

distributed microbubbles, nanobubbles can achieve a higher agent density in the vessel [39], providing more interaction sites for cell-specific targeting (**Figure 1E**), and/or potentially increase the payload capacity due to an increased surface area to volume ratio for ultrasound-stimulated therapies. Owing to the increased bubble concentration *in situ*, nanobubbles can also be associated with enhanced tumour drug uptake [40] upon ultrasound stimulation, leading to improved therapeutic efficacy (**Figure 1F**).

Designing nanobubbles to specifically respond to ultrasound at clinical frequencies and at pressures safe for normal tissue requires additional considerations compared to the development of more stable solid or liquid-phase nanoscale agents. Nanobubbles are fundamentally different from conventional nanoscale agents as their highly compressible gas cores and pliable shells can be acoustically driven to vibrate, the primary mechanism of interaction with ultrasound. Although the concept of nanobubbles for medical ultrasound has been included as part of wider ultrasound bubble-based contrast agent reviews in the past [29, 41–43], the basic design considerations particular to nanobubble formulations intended for clinical medical imaging and therapy applications have yet to be addressed. Specifically, we will first introduce the physics of bubble vibration and highlight the potential advantages of scaling down from microbubbles to nanobubbles, from both an imaging and therapeutic viewpoint. Next, we will discuss development criteria of lipid-encapsulated nanobubbles such that they can eventually meet clinically meaningful endpoints; from agent synthesis and characterization to *in vivo* considerations. Finally, our concluding remarks discuss future opportunities of nanobubbles for new and emerging applications in medicine.

IMPACT OF BUBBLE SIZE ON ACOUSTIC AND BIOLOGICAL PROPERTIES

Nanobubble contrast agents require their physical properties, including their size, to be concurrently optimized with their acoustic and biological properties for successful imaging or treatment. In this section, the fundamental impact of bubble size in relation to ultrasound interactions will be briefly introduced, followed by the implications arising from scaling down bubble size to the nanoscale. For a more complete analysis of acoustically-driven bubble dynamics, the reader is referred to recent review articles [44, 45].

Size-Dependent Bubble Vibration Physics

Within an ultrasound field, a gas bubble of initial radius R_0 exhibits a linear undamped resonance frequency f_0 given by:

$$f_0 = \frac{1}{2\pi}\sqrt{\frac{1}{\rho R_0^2}\left(3\gamma P_0 + \frac{2\sigma_0\,(3\gamma - 1)}{R_0} + \frac{4\chi}{R_0}\right)} \qquad (1)$$

where ρ is the fluid density, γ is the polytropic index, P_0 is atmospheric pressure, σ_0 is the initial surface tension at the gas-liquid interface, and χ is the shell elasticity. As can be seen from the above equation, there is an inverse relationship between bubble size and resonance frequency. Using a typical value for lipid shell elasticity (0.5 N/m [44]), microbubbles between 2 and 8 μm in diameter exhibit a resonant frequency f_0 that falls within 1–10 MHz, commonly used in clinical imaging. Scaling down bubble size toward the nanobubble range (diameters 0.2–0.8 μm) results in a drastic increase in resonance frequency (∼30–250 MHz) which lies well-outside of the clinically employed frequency range. Despite this, there have been recent studies highlighting scattering from nanobubble formulations at off-resonant (i.e., clinically relevant) frequencies (1–10 MHz; e.g., [46, 47]).

The observed strong acoustic response from nanobubbles at clinical frequencies is unexpected from conventional cavitation models, but may begin to be rationalized using several explanations. For example, it is important to note that a decrease in radius confers an increase in bubble density within a fixed ultrasound focal volume. As the bubble radius decreases by a factor of x, this results in an x^3-fold increase in bubble density which may offset the weaker scattered signal on a single bubble basis. Second, it is essential to consider the complete non-linear radial response—likely influenced by the encapsulation rheology. In addition to other sources, the shell contributes strongly to bubble vibration damping, scaling as $\frac{1}{R_0^3}$ and thus plays an increasingly significant role as bubble size decreases. The resulting damped resonance frequency f_{res}, which is the frequency at which there is a maximum radial response, diverges significantly from f_0 as $R_0 < 1\,\mu$m. This results in much lower resonance frequencies ($f_{res} < 50$ MHz) or even an overdamped system, whereby a local maximum in frequency response is lost. Such vibrations and subsequent scattering from nanobubbles at more clinically relevant frequencies may be made possible due to the inherent non-linearities due to shell encapsulation material physics. As has been shown for small microbubbles (∼1–2 μm), off-resonance bubbles can be made to exhibit strong non-linear signal owing to the shear-thinning and/or strain-softening rheology of the lipid encapsulation [48, 49] as well as transmit-pressure dependent resonance characteristics [50]. Subharmonic and ultra-harmonic scattering can thus be initiated at transmit frequencies well-below resonance ($f \sim$ 0.2–0.5f_0) which lie closer to clinical frequencies. However, our current understanding of nanobubble physics assumes nanoscale shell rheology that is similar to that which has been quantified on the micrometer-scale. Further elucidation of the mechanism behind the strong non-linear acoustic response of nanobubbles will need to be verified experimentally in future studies. This will include comprehensive nanobubble encapsulation characterization and the specific shear and strain-dependent relationships of the shell under megahertz oscillations.

Advantages of Scaling From Microbubbles to Nanobubbles *in vivo*

Increased Acoustic Response at Higher Frequencies and/or Higher Agent Concentrations Due to Smaller Bubble Size

Although nanobubbles have been shown to respond non-linearly to ultrasound at relatively low frequencies (f ∼1–10 MHz),

bubbles are still expected to have stronger acoustic responses closer to their resonance frequencies (e.g., f_{res}). Thus, perhaps the most direct advantage of scaling down the size of bubbles from the micrometer to nanometer range is their increased echogenicity in high-frequency contrast applications ($f > 15$ MHz), including breast imaging [51] and small animal imaging [52]. Another application may be in intravascular ultrasound (IVUS; $f \approx 20 - 50$ MHz), whereby a catheter incorporating a miniature transducer is placed within blood vessels to acquire cross-sectional images of arteries to assess lesion severity and plaque morphology in patients with suspected coronary artery disease [53, 54]. Contrast-enhanced IVUS has been shown as a reliable approach to detect the *vasa vasorum*, a network of small blood vessels that supply the larger vessel walls, the pathological development of which has been linked with plaque progression [55, 56]. Further, combining targeted bubbles with IVUS holds considerable promise as a means to gain insight into the molecular status of atherosclerotic plaques [57].

As the transmit frequency increases, the focal volume decreases, thus limiting the available number of bubbles that are sensitive to the acoustic beam. Scaling the bubble size down to hundreds of nanometers can potentially increase image quality beyond initiating bubble vibration closer to its natural resonance. Indeed, for a fixed volume of gas, the number of nanobubbles will be greater than the number of microbubbles. Using clinically approved microbubble agents as an example (e.g., SonoVue^{TM}; $d_{peak} \approx 4 - 5\mu m$ [58], Sonazoid^{TM}: $d_{peak} \approx 3\mu m$ [59]), this represents a relative increase of approximately 10^3-fold in number concentration for nanobubble agents ($d_{peak} \approx 250$ nm [41]). This increased number of acoustic sources in a focal volume using nanobubbles compared to microbubbles can result in a higher overall acoustic response.

In a similar fashion, an increased bubble number density also has potential advantages in ultrasound-assisted drug/gene delivery applications [23]. For such applications (e.g., cancer [60], cardiovascular disease [61]), therapeutic payloads are often conjugated to the surface of the bubble and thus exhibit a loading capacity proportional to R^2. Given that the surface area to gas volume ratio increases with decreasing bubble size, so too does the total drug loading capacity, potentially leading to increased therapeutic efficacy.

Unique Biological Interactions Arising From Size-Dependent Agent Biodistribution and Accumulation *in vivo*

Imaging pathophysiological processes at their molecular level can be used to detect disease at a very early stage, well-before anatomical changes are observed. Molecular imaging can also assess the spatial extent and severity of disease, as well as guide therapeutic treatments. Through exploitation of differential kinetics of bound vs. unbound, freely circulating bubbles, techniques have been established to estimate contrast signal due solely to targeted bubbles and therefore generate disease-specific images [62]. While current approaches using microbubbles have been shown to detect disease in preclinical models, the comparatively large microbubble size relative to its intended biomarker confounds the link between bound bubble response and targeted molecular expression level. This presents a limitation in quantifying biomarker expression, as the resulting bubble echo is not necessarily linearly proportional to molecular density. As the targeted bubble scales down to the nanoscale, a bubble can represent a more direct surrogate for molecular expression as it becomes closer in size to target biomolecules. Further, under the assumption that agent dose is limited by gas volume fraction [63], the increased nanobubble concentration compared to its microbubble counterpart has the potential to more finely spatially sample the diseased region and provide more accurate estimates on spatial extent. Indeed, there are ongoing preclinical investigations using intravascularly targeted nanobubbles toward VEGFR2 [64, 65] and ICAM-1 [66]. Under pathological conditions, for example in cancerous sites where tumour microvessels are known to be more permeable [7], nanobubbles may have the unique opportunity to exit the vasculature and thus extend the utility of ultrasound molecular imaging to beyond the intravascular space. The feasibility of molecular imaging of overexpressed extravascular cell targets has been reported in preclinical models using nanobubbles targeted to cancer antigen 125 (CA-125; [67]), HER2 [68], prostate specific membrane antigen [69], G250 [70] as well as T-cell markers CD25 [71] and CD3 [72] for clinical immune surveillance of transplant rejection.

In addition to imaging new molecular targets with ultrasound, vibrating gas bubbles within the extravascular tumour microenvironment may aid in anticancer drug distribution and efficacy. The tumour microenvironment hinders intravascular drug delivery due to a variety of factors, including large distances between vessels in solid tumours, the extracellular matrix composition, high interstitial fluid pressure, and lack of convection (e.g., [73]). If nanobubbles can accumulate within the extravascular compartment, they can leverage the well-established ability of acoustically driven gas bubbles to modify the fluid flow in their immediate vicinity (e.g., microstreaming [74]) and, under specific acoustic conditions, generate high-velocity fluid jets [75]. This local fluid mixing is hypothesized to aid in drug penetration within solid tumours. Also, similarly to microbubbles, nanobubbles can be decorated with drug or molecular therapeutics on their lipid shell [76], but without the requirement of the drug payload passing across the endoluminal border to the diseased tissue. As nanobubbles can be in direct contact with extravascular diseased cells, drug penetration and intracellular access to these cells in therapeutically relevant concentrations may be improved in comparison to microbubbles, which can lead to improved drug efficacy [77].

DEVELOPMENT OF LIPID-ENCAPSULATED NANOBUBBLES: SYNTHESIS AND VALIDATION

Despite clear opportunities presented by nanobubbles and recent advances in biomaterials engineering, new nanobubble development is at a relatively early stage compared to the development of their microbubble counterparts and other types

of nanoscale agents (solid or liquid-based colloidal agents). A variety of nanobubbles that range widely in size (∼200–800 nm), shell material (e.g., polymer, phospholipids, protein) and core gas (e.g., air, perfluorocarbon, sulfur hexafluoride) have been demonstrated in basic science and preclinical literature [29, 30, 43, 78–85]. It is expected that, similar to microbubbles [38, 44, 86], the effect of nanobubble composition, size distribution, and concentration will impact the agents' *in vivo* performance in both imaging and therapy, as well as their manufacturability, cost, and eventual approval for clinical use [42]. Due to the compositional similarity to approved microbubbles formulations, we focus on overviewing fluorocarbon gas-filled, lipid-stabilized nanobubble variants. These nanobubbles are considered as strong candidates for translation into human patients, can more easily fit into established clinical workflows and can be used with ultrasound systems that are already commonplace [11, 42, 86]. In this section, the main physical properties of nanobubbles and methods used to characterize them will be introduced.

Nanobubble Synthesis Methods

Ultrasound contrast agents used in the clinic today are commercially available microbubbles that primarily come in two forms: (1) in a vial consisting of an aqueous solution containing the shell material (e.g., phospholipids and excipients) that is "activated" via a companion vial shaker, or (2) a vial composed of a lyophilized phospholipid cake that is reconstituted with saline. In both cases the headspace of the vial is filled with a high-density gas, and the bubbles are activated on-site. The on-site preparation of the bubble agent adds a minor barrier to clinical implementation, but this permits more structurally and acoustically consistent populations of bubbles to be injected across different patients. To further reduce potential changes in the bubbles that occur over time, the resulting polydisperse bubbles are typically injected into a patient within several hours post-activation. The polydispersity of commercial bubbles permits their use over a wide range of frequencies and potentially longer imaging times, as larger bubbles shrink into the size range where they are resonant with the ultrasound field to backfill resonant bubbles that fall out of the same size range. However, the polydispersity of bubbles makes quantitative and longitudinal imaging difficult, as extraction of similar sized bubbles from vial to vial is strongly dependent on agent handling [87].

In the literature, nanobubbles are typically prepared using a variety of methods. For example, researchers have prepared nanobubbles by isolating the submicron population of polydisperse microbubbles, either from post-activated commercial microbubble products [47] or, for those with the appropriate expertise and infrastructure, from microbubbles prepared in-house using well-established sonication or agitation procedures that have been extensively characterized *in vivo* [86]. Isolation of the sub-micron population from polydisperse microbubbles can be accomplished via centrifugation [88], or floatation and filtration [87]. The advantages of these techniques are 2-fold: firstly, the relatively simple procedures do not require any modification of well-established bubble formulations. Secondly, these nanobubbles are not expected to result in any biocompatibility issues *in vivo*. Consideration must be given to the fragile nature of the bubbles themselves: the isolation procedure may alter the bubble properties—including bubble collapse, coalescence, fragmentation, and liposome formation, which can be bubble size-dependent [38]. Centrifugation speeds, for example, must be carefully chosen to avoid these destructive effects. In addition, the isolation procedure is time sensitive as the bubbles may change as a function of time, notably when native bubble solutions are diluted. This may lead to challenges in bubble population reproducibility between different users and labs.

Other researchers have attempted to synthesize nanobubbles directly. One such example is the formation and hydration of thin lipid films followed by agitation with fluorocarbon gas, similar to the process used to form clinical lipid microbubbles (e.g., Definity^{TM}). This approach, in combination with size and stability controlling excipients [46, 67, 82] has the advantage of synthesizing a starting population of bubbles with a size distribution that is largely submicron. From this stage, these nanobubbles can be further manipulated to select bubbles with an even more narrow size distribution. From a clinical standpoint, any requirement for atypical, user-dependent, on-site processing of the nanobubbles has the potential to add variability to the agent population, which may ultimately reduce performance. An alternative option may be to lyophilize a pre-isolated population of size-stratified nanobubbles to minimize on-site bubble variability prior to clinical use [59]. It should be noted that any new modification of the formulation either using novel lipid mixtures or by changing the concentration of bubble components will require revalidation of its *in vivo* stability and performance, which can be an extensive undertaking.

Along with bubble size, bubble shell properties play a large role in their vibration and scattering dynamics. It has been demonstrated that microbubbles formed via the above approaches, even when size and formulation-matched, can exhibit heterogeneous acoustic responses on a single bubble level [89], possibly due to the initial state of the phospholipid encapsulation. An emerging technique of bubble synthesis using micro/nanofluidic systems offers the potential for further bubble size control and encapsulation homogeneity. However, early work has resulted in the mixed production of both nanobubbles and nanodroplets [90], and the concentration and yield using current on-chip generation of nanobubbles is not yet sufficient for patient use. Studies and technical developments to address these barriers are ongoing [42].

Physical Characterization of Nanobubbles

Nanobubble formulations are typically characterized by their size distribution and concentration over time (stability). Microbubbles are designed to be rapidly broken down and harmlessly cleared from the patient post-imaging, typically within minutes post-injection. Nanobubbles need to be stable enough to be imaged over the time required to reach the site of interest, which can occur over time periods ranging from minutes (for blood pool imaging or to reach endothelial targets) or many hours (to accumulate within tumours). Thus, the stability of the agent, which is highly dependent on the nanobubble formulation, is a critical parameter that must be engineered

for its intended application. The combination of buoyancy and instability of nanobubbles complicates the characterization of this agent in comparison to other nanoscale agents (e.g., nanoparticles, liposomes or micelles).

Perhaps the most reliable, repeatable and widespread method for physical characterization of microbubbles is resistive pulse sensing (RPS), otherwise known as the Coulter Principle. This technique measures both the size distribution and concentration of bubbles based on the electrical response as they pass through a sensing zone. Bubble buoyancy is less of an issue with this approach due to the relatively short measurement duration and forced flow. For scaling this approach toward characterizing nanobubbles, a fundamental limitation is particle size sensitivity, determined by the size of the measurement aperture. Recent development of a 10 μm aperture (Coulter Counter Multisizer 4e) allows for a minimum measurable nanobubble size of ∼200 nm, sufficient for early-stage nanobubble formulation stability assessment. Dynamic light scattering (DLS), also known as photon correlation spectroscopy, estimates population size distribution from the fluctuations of scattered light and the Stokes-Einstein relation. This technique can measure minimum sizes of ∼1 nm but cannot quantify particle concentration. Although DLS may be suitable for relatively monodisperse solid or liquid nanoscale agents, the size-dependent buoyancy of bubbles can lead to inaccurate measurements as larger bubbles float faster out of the field of view of the DLS laser compared to smaller bubbles. Nanoparticle tracking analysis (NTA), which uses similar physics as the DLS principle to visually track the Brownian motion of nanoparticles, has the added advantage of being able to estimate particle concentration but suffers a similar problem to DLS as the bubbles move in and out of the imaging field. The use of optical microscopy in combination with a hemocytometer for nanobubble concentration and size measurements has been reported, but as many nanobubbles are below optical resolution limits, these measurements skew toward the assessment of larger bubbles. Electron microscopy has been used to estimate nanobubble size, but since nanobubbles exist in the form of an aqueous suspension, the sample must be dried or frozen (e.g., for cryo-EM) prior to its characterization, which can be technically challenging for fragile bubbles. While these approaches have distinct advantages and disadvantages, they can provide complementary information on physical nanobubble characteristics and multiple approaches can be employed to corroborate individual findings.

Synthesizing nanobubble agent can result in populations that can be a mixture of nanobubbles, liposomes, and nanodroplets [90, 91], and many of these measurement techniques cannot differentiate these populations from each other. Resonant mass measurement techniques (e.g., Archimedes, Malvern), whereby a resonating cantilever device measures the relative size, mass, and concentration of samples, has recently been proposed as a means to separate buoyant (e.g., bubbles) from non-buoyant particles. Aside from this technique, centrifugation may be used to separate different nanoscale populations with different densities, and bubble destructive techniques (e.g., intentional inertial cavitation of the bubble population) can be used to assess differences in pre- and post-burst populations and thus validate nanobubble presence in the initial population.

Given that the encapsulating shell plays a large role in non-linear bubble vibrations [44], information on the composition and molecular organization of the phospholipids and excipients in the nanobubble shell is critical, yet not easily determined. Our current understanding of nanobubble encapsulation has been extrapolated from previous work on microbubbles, e.g., using fluorescently labeled lipids and using fluorescence microscopy [92], which cannot easily be performed on nanoscale agents. Alternatively, isolation of nanobubbles from aqueous solution in combination with NMR can potentially identify shell components [93], but this technique will not reveal the spatial arrangement of the lipids and individual bubble-to-bubble consistency. The assessment of drug loading yield and targeting potential can be conducted using techniques similar to those used for microbubble assessment (e.g., ultraperformance liquid chromatography and mass spectrometry, toxicity assays, and cell targeting assays [42]), with the caveat that isolation and identification of the nanobubbles from non-bubble structures can be more challenging in comparison to larger, more buoyant microbubbles.

Acoustic Assessment of Nanobubbles

The eventual utility of nanobubbles requires their acoustic properties to be well-characterized *in vitro* and *in vivo*. By design, nanobubbles are fragile to facilitate their *in vivo* clearance and on-demand acoustic disruption. The techniques and salient acoustic readouts for nanobubble populations are in principle similar to those of microbubbles. Care must be taken, however, to ensure that the population of nanobubbles does not contain microbubble outliers, as these can significantly affect the acoustic readouts. The scattered pressure P_s from a single bubble is strongly size-dependent, the behaviour of which depends on the transmit frequency f in relation to the value of the natural resonance frequency f_0 of the bubble. According to conventional linear acoustic cavitation theory (Eq. 1), a nanobubble insonated at clinical frequencies ($f \approx 1-10$ MHz) is being driven well-below its resonance frequency ($\frac{f}{f_0} \ll 1$); namely the bubble is much smaller than the resonant size for the given ultrasound field. In this instance, the scattered pressure at a location r from an individual unencapsulated bubble of size R_0 tends toward the following expression:

$$P_s \rightarrow P_{ac}\frac{\rho\omega^2 R_0^3}{3\gamma p_0 r}, \tag{2}$$

where P_{ac} is the transmit pressure amplitude, $\omega = 2\pi f$, and p_0 is atmospheric pressure. In comparing, for example, the scattered pressure from a nanobubble of size R_n and a microbubble of size $R_m = 10R_n$, it can be readily shown that the microbubble contribution is on the order of 10^3 times larger than that of the nanobubble—under the assumption that the microbubble is also driven below resonance (i.e., that Eq. 2 holds). However, it is well-established that the resonance frequency of a typical microbubble falls within the clinical frequency range. When driven near

resonance $\frac{f}{f_0} \cong 1$, the scattered pressure approximates to

$$P_s \rightarrow P_{ac} \frac{\rho \omega R_0^3}{4\mu_l r}, \tag{3}$$

where μ_l is the viscosity of the surrounding fluid. Under such circumstances, where the microbubble is driven near resonance (Eq. 3), the nanobubble will still be driven below resonance (Eq. 2). It can easily be shown that with a factor of 10 in size increase from nanobubble to microbubble, the scattered pressure contribution from the "contaminating" microbubble can be on the order of 10^4 times greater than its nanobubble counterpart. Although this is a comparison between a single microbubble and a single nanobubble, it is clearly important to make accurate correlative measurements of nanobubble size and concentration to interpret the corresponding acoustic evaluations.

Indeed, there are two main groups of acoustic bubble population characterization experiments. Frequency-dependent attenuation measurements consist of a substitution method, whereby the echo from a planar reflector is recorded with and without bubble populations within the beam path. Under low amplitude driving conditions (to avoid bubble disruption and minimize non-linear echoes) with dilute samples (to safely ignore multiple scattering effects), the frequency at which peak attenuation occurs corresponds to the low-pressure resonance frequency of the bubble population [87]. In conjunction with size distribution information, this dataset can also be used to estimate linearized shell parameters (e.g., [94]), in furtherance of encapsulated bubble modeling and design efforts. Scattering experiments, conducted either within water-based, tissue-based or tube-like phantoms to mimic the vasculature, are employed to assess non-linear acoustics, including higher order harmonics (nf where $n = 2, 3, 4, \ldots$), subharmonics ($nf/2$ where $n = 1, 3, 5 \ldots$), and wideband emissions, the latter of which is well-known to correspond to bubble disruption. Assessment of the non-linear scattering of bubbles is an essential feature of their acoustic characterization since harmonic signal content is exploited to generate bubble-specific contrast images, with specific emphasis on subharmonic emissions as they do not suffer from non-linear acoustic propagation artefacts. While bubble disruption can be used for high-powered flash imaging protocols, it is also an important feature in targeted drug-delivery applications where it can potentially be used to release attached therapeutic cargo. As such, these acoustic measurements are usually performed as a function of frequency and transmit pressure to assess the range of acoustic conditions able to initiate the desired acoustic activity.

Comprehensive optical microscopy, scattering and theoretical modeling work has shed insight into the critical non-linear behaviours of individual microbubbles, including "compression-only" oscillations [95], shell surface rheology effects [96], non-linear resonance [50], and the onset of vibration [48], all of which have increased our understanding of contrast agent design and optimization. However, comparable investigation into the non-linear dynamics and associated scattering of single nanobubbles remains a challenge due to their size. *In-vitro* acoustic measurements using tone bursts on populations of nanobubbles at clinical and high frequencies (up to 30 MHz) have recently provided evidence of non-linear scattering [47, 97], and contrast imaging of nanobubble populations has been demonstrated using clinical [41, 98–103] and pre-clinical scanners [90, 104]. Collectively, these works have demonstrated that, similar to their micron-sized counterparts, nanobubble populations exhibit the capacity to initiate sustained non-destructive harmonic and subharmonic scattering that is transmit pressure-dependent, as well as undergo ultrasound-induced bubble disruption at high driving amplitudes.

In vivo Considerations

Although there are significant limitations with preclinical systems as accurate models of human disease, the use of preclinical models is a critical step toward optimizing and validating a nanobubble formulation for future clinical translation. While early work has reported the feasibility of nanobubble imaging and therapeutic approaches [64–70, 72, 78, 80, 82–85, 105–107] using *in vivo* models of disease, we highlight here some critical factors that may affect nanobubble characterizations *in vivo* and their interpretation.

It should be noted that agent handling can be a large source of variability, as different techniques for bubble activation [94] and withdrawal [87] can lead to alternative size distributions and subsequent acoustic activity. Firstly, it is important to use a secondary venting needle upon agent extraction [108], and careful consideration should be given to proper bubble injection techniques, including the size of the extraction needle and injection rate, both of which have been shown to significantly affect bubble stability *in vivo* in imaging [109] and therapeutic contexts [110]. Secondly, differential floating of bubble solution will modulate the resulting bubble concentration and size distribution, and therefore bubble suspensions (e.g., in a syringe) should be well-mixed prior to injection. Given the smaller size as compared to microbubbles, nanobubble floatation is expected to occur on much longer timescales and may be a less important factor. It is also important to consider physiological effects on bubble stability. The potential influence of the choice of animal anesthesia has been shown to affect bubble *in vivo* circulation times [111], and bubble behaviour (e.g. scattering) is likely affected by ambient body temperature [112]. Finally, since the nanobubble response depends on the transmit ultrasound conditions, careful consideration should be given to the ultrasound system and associated transducers employed. Nanobubble imaging studies, including development of novel pulse-sequences or disease-detection techniques, for example, can be conducted with a preclinical scanner with the understanding that the imaging signal may not be equivalent to what will be achievable with a clinical scanner.

With respect to target nanobubble concentrations, it is perhaps instructive to compare these agents with clinically used microbubble agents. Activated Definity^{TM}, for example, is characterized by a mean number-weighted microbubble size of 1.1 μm, a native concentration of $\sim 10^{10}$ bubbles/ml and consists of 150 μL of perfluorocarbon gas per ml [113]. The recommended maximum bolus dose of activated Definity^{TM} is 20 μL per kg, resulting in 3 μL of perfluorocarbon per kg. A reasonable starting point for nanobubble dosing is to assume that

the recommended injected gas volume remains constant between microbubble and nanobubble formulations. Given a nanobubble distribution characterized by an average bubble size of $R_n = 150$ nm, this constant gas volume can be approximately maintained with a 20 μL per kg injection of a native nanobubble solution that is a factor of 10^3 times more concentrated than current clinical microbubble agents ($\sim 10^{12} - 10^{13}$ nanobubbles/mL). While in principle an increased concentration yields a stronger acoustic signal, the inter-bubble spacing ($\approx 0.5 - 1$ μm) at such high concentrations may result in multiple scattering [114] and bubble coalescence effects [115] (i.e., fusing of smaller nanobubbles into bigger micron-sized bubbles), which may partially negate the intended benefit of nano-sized agents.

OUTLOOK

New and emerging applications of ultrasound have arisen from exciting developments in application-specific devices and, in parallel, from increasing clinical awareness of opportunities that ultrasound technologies can bring to medical practice. This growing integration between basic scientists, engineers and medical practitioners has led to innovative technologies designed to meet nuanced clinical needs for rapid translation to patients, and similar approaches may lead to novel nanobubble development. Several examples of potential opportunities in nanobubble-assisted ultrasound applications are given below.

Ultrafast Plane Wave Imaging

A flourishing area is ultrafast ultrasound imaging [116], in which up to 20 kHz frame rates (compared to 10–100 Hz using conventional scanners) can be achieved through advances in hardware and software. This technology has opened up the field to an array of contrast and non-contrast applications to take advantage of the increased temporal resolution, including ultrafast elastography [117], cardiac [118], and Doppler-based applications [119]. In particular, ultrasound localization microscopy (i.e., super-resolution imaging [120]) exploits the localization of microbubbles to finely sample and image the microcirculation beyond the diffraction limit; a technique that has shown impressive results in the areas of oncology (e.g., [121]) and neurology (e.g., [122]). A nanobubble adapted version of this technique could open further avenues other than vascular-based imaging, including the observation and mapping of the interstitial microenvironment and the temporal assessment of nanoscale agent accumulation outside leaky vessels.

Ultrasound-Assisted Neuromodulation

Neuromodulation is the process of altering neural behaviour through stimulation or suppression of nerve activity. Focused ultrasound is an emerging non-invasive technique with tremendous potential as a novel neuromodulation tool, with advantages over current clinical approaches (e.g., deep brain stimulation, transcranial electric/magnetic stimulation) that include its non-invasiveness, site-specific targeting and the ability to interrogate deep regions in the brain [123]. This technique, generally performed under MRI-guidance, achieves a focal region of acoustic pressure through constructive interference at depth in the brain without affecting tissue along its focal path closer to the transducer array, leading to various bioeffects of differing physical origin. Depending on the ultrasound parameters, focal tissue thermal ablation can be induced and has application in brain cancers, as well as tremors in order to improve symptoms and patient outcome [123]. The closely-related field of ultrasound and microbubble mediated transient opening of the blood-brain-barrier can be achieved likely via mechanical mechanisms, where this increased permeability provides a controllable and reversible opportunity for targeted delivery of therapeutics [124]. Additionally, lower intensity ultrasound alone can achieve direct neuromodulation of neurons without therapeutics or contrast agents in both animal and human models [123], the mechanisms of which remain largely unexplored. Nanobubbles present an exciting new opportunity to enhance and/or synergize ultrasound-assisted neurology techniques. First, compared to ultrasound alone, nanobubble cavitation is expected to increase local shear-stress profiles and may offer a more spatially sensitive approach to activation of mechanosensitive ion channels present within cell membranes. Second, the increased loading capacity compared to microbubbles may provide a more efficient means of therapeutic delivery to the brain parenchyma—with or without necessitating ultrasound-mediated blood-brain-barrier disruption depending on the molecular size of the neuromodulating therapeutic. Indeed, ultrasound-assisted neuromodulation using nanometer-sized acoustically sensitive agents has been very recently demonstrated [125, 126].

Ultrasound-Assisted Immunotherapy

Cancers can evade immunosurveillance and circumvent the normal immune response through a variety of mechanisms, including ineffective presentation of neoantigens on tumour cell membranes, a lack of signaling to activate naïve T-cells, and a physiologically hostile tumour milieu. In general, cancer immunotherapy approaches aim to modulate immune responses to further increase anti-cancer cell targeting and killing, the main categories of which include immune checkpoint inhibitors (CTLA-4 and PD-1/PD-L1 antibodies) and cellular immunotherapies (e.g., chimeric-antigen receptor T cells) [127]. While met with initial success, the current limitations of this approach include off-target side effects and sub-optimal tumour penetration. Novel ultrasound-assisted immunotherapy approaches are rapidly being developed to address this [23, 128]. Specifically, emerging research in microbubble-assisted ultrasound approaches has demonstrated exciting potential to improve anti-PD-1 antibody delivery [129], enhance lymphocyte infiltration to the tumour interstitium [130], and promote key interleukin secretion within the tumour microenvironment [131]. Nanobubble agents may have a complementary role to play in further promoting these effects due to their potential to extravasate within tumour tissue; either passively or actively through concurrent sonoporation techniques. The increased proximity of nanobubbles to target cancer cells may improve these immunomodulating techniques compared to their larger microbubble counterparts.

Concluding Remarks

Beyond the applications described above, as more cutting-edge ultrasound-focused developments and greater understanding of disease biology occur, so too will the opportunities for nanobubbles. New disease targets and applications for nanobubbles are continually being reported (e.g., detecting insulitis in type 1 diabetes [78]). Cavitation of nanobubbles may result in a mixture of end products, including more stable liposomes, micelles, and aggregates which may be therapeutically advantageous [132]. In addition, there are numerous specialized ultrasound imaging and therapy platforms that are typically not used with contrast, yet can be adapted for contrast imaging or for local therapeutic delivery. These include catheter-based endobronchial ultrasound for thoracic imaging [133], external MRI-guided focused ultrasound systems to treat bone metastases and uterine fibroids [134, 135], and insertable ultrasound probes for treatment of prostate cancer [136] or the heart [137]. Since these systems can allow focused ultrasound to reach parts of the body that are less accessible to standard ultrasound systems, there is an opportunity to leverage this access to treat diseases using new nanobubble constructs tailored to the technological specifications of the ultrasound system. Although most bubble-based agents have been focused on imaging or treating cancer, inflammation or heart disease, applications of bubbles and ultrasound have greatly expanded to include use ranging from infection control [138, 139] to radiosensitization [140] and non-invasive liquid biopsy [141, 142]. Nanobubbles have also been proposed as a more acoustically responsive analogue to nanodroplets, for thermal sensitization for radiofrequency treatment [143], ameliorating hypoxia [144], and potentiating photodynamic therapy [43]. Indeed, in principle, nanobubbles possess certain advantages over nanodroplets, including native echogenicity and lower cavitation thresholds.

It is clear that the recent development of nanobubble agents has led to exciting possibilities and numerous emerging opportunities for future exploration. The continued development of new nanobubble variants, novel nanoscale synthesis methods, improved nanoscale characterization, and more efficient targeting methods is expected to considerably advance the utility of contrast-assisted ultrasound imaging and therapeutics. This will undoubtedly lead to new fundamental discoveries in ultrasound physics, materials chemistry, and clinical medicine.

AUTHOR CONTRIBUTIONS

BH and NM co-led the scientific research and writing of the full paper. NM is the corresponding author of the article. YZ contributed partly to the writing of the overview section of the paper. All authors contributed to the article and approved the submitted version.

FUNDING

This work was supported, in part, by Prostate Cancer Canada, the Movember Foundation (D2014-7), and the Ontario Research Fund, Early Researcher Award (ER14-10-178), the Canadian Cancer Society (703909), the Natural Sciences and Engineering Research Council of Canada (2015-05835 & 2019-06969), the Fonds de Recherche du Quebec, the CFI-JELF program (36586), the University of Toronto EMHSeed Program, the Ontario Research Fund–Research Excellence Program, the CIHR Project Scheme (426350), and the New Frontiers in Research Fund–Exploration (2019-00256). BH holds a Career at the Scientific Interface award from the Burroughs Wellcome Fund (BWF-CASI).

ACKNOWLEDGMENTS

The authors would like to thank Dr. Carly Pellow and Mr. Ross Williams for their help revising the manuscript. Figure was created with BioRender.com.

REFERENCES

1. Szabo TL. *Diagnostic Ultrasound Imaging: Inside Out*. Oxford: Elsevier/Academic Press (2014).
2. Cobbold RSC. *Foundations of Biomedical Ultrasound*. New York, NY: Oxford University (2007).
3. Correas JM, Anglicheau D, Joly D, Gennisson JL, Tanter M, Hélénon O. Ultrasound-based imaging methods of the kidney—recent developments. *Kidney Int*. (2016) 90:1199–210. doi: 10.1016/j.kint.2016.06.042
4. Spencer KT, Kimura BJ, Korcarz CE, Pellikka PA, Rahko PS, Siegel RJ. Focused cardiac ultrasound: Recommendations from the american society of echocardiography. *J Am Soc Echocardiogr*. (2013) 26:567–81. doi: 10.1016/j.echo.2013.04.001
5. Jahromi AS, Cinà CS, Liu Y, Clase CM. Sensitivity and specificity of color duplex ultrasound measurement in the estimation of internal carotid artery stenosis: a systematic review and meta-analysis. *J Vasc Surg*. (2005) 41:962–72. doi: 10.1016/j.jvs.2005.02.044
6. Sehgal CM, Weinstein SP, Arger PH, Conant EF. A review of breast ultrasound. *J Mammary Gland Biol Neoplasia*. (2006) 11:113–23. doi: 10.1007/s10911-006-9018-0
7. Folkman J. Angiogenesis: an organizing principle for drug discovery? *Nat Rev Drug Discov*. (2007) 6:273–86. doi: 10.1038/nrd2115
8. Khurana R, Simons M, Martin JF, Zachary IC. Role of angiogenesis in cardiovascular disease: a critical appraisal. *Circulation*. (2005) 112:1813–24. doi: 10.1161/CIRCULATIONAHA.105.535294
9. Carmeliet P. Angiogenesis in life, disease and medicine. *Nature*. (2005) 438:932–6. doi: 10.1038/nature04478
10. Lindner JR. Microbubbles in medical imaging: current applications and future directions. *Nat Rev Drug Discov*. (2004) 3:527–32. doi: 10.1038/nrd1417
11. Sirsi SR, Borden MA. Microbubble compositions, properties and biomedical applications. *Bubble Sci Eng Technol*. (2009) 1:3–17. doi: 10.1179/175889709X446507
12. Medwin H. Counting bubbles acoustically: a review. *Ultrasonics*. (1977) 15:7–13. doi: 10.1016/0041-624X(77)90005-1
13. Brock-Fisher GA, Poland MD, Rafter PG. *Means for Increasing Sensitivity in Non-Linear Ultrasound Imaging Systems*. Patent number: US5577505A (1996). doi: 10.1121/1.418339
14. Simpson DH, Chin CT, Burns PN. Pulse inversion Doppler: a new method for detecting nonlinear echoes from microbubble contrast

agents. *IEEE Trans Ultrason Ferroelectr Freq Control*. (1999) 46:372–82. doi: 10.1109/58.753026
15. Wei K, Jayaweera AR, Firoozan S, Linka A, Skyba DM, Kaul S. Quantification of myocardial blood flow with ultrasound-induced destruction of microbubbles administered as a constant venous infusion. *Circulation*. (1998) 97:473–83. doi: 10.1161/01.CIR.97.5.473
16. Hudson JM, Karshafian R, Burns PN. Quantification of flow using ultrasound and microbubbles: a disruption replenishment model based on physical principles. *Ultrasound Med Biol*. (2009) 35:2007–20. doi: 10.1016/j.ultrasmedbio.2009.06.1102
17. Porter TR, Feinstein SB, Ten Cate FJ, van den Bosch AE. New applications in echocardiography for ultrasound contrast agents in the 21st century. *Ultrasound Med Biol*. (2020) 46:1071–81. doi: 10.1016/j.ultrasmedbio.2020.01.004
18. Barr RG, Wilson SR, Lyshchik A, McCarville B, Darge K, Grant E, et al. Contrast-enhanced Ultrasound-State of the Art in North America: Society of Radiologists in Ultrasound White Paper. *Ultrasound Q*. (2020) 36:S1–S39. doi: 10.1097/RUQ.0000000000000515
19. Klibanov AL. Preparation of targeted microbubbles: ultrasound contrast agents for molecular imaging. *Med Biol Eng Comput*. (2009) 47:875–82. doi: 10.1007/s11517-009-0498-0
20. Lentacker I, De Cock I, Deckers R, De Smedt SC, Moonen CTW. Understanding ultrasound induced sonoporation: definitions and underlying mechanisms. *Adv Drug Deliv Rev*. (2014) 72:49–64. doi: 10.1016/j.addr.2013.11.008
21. Qin P, Han T, Yu ACH, Xu L. Mechanistic understanding the bioeffects of ultrasound-driven microbubbles to enhance macromolecule delivery. *J Control Release*. (2018) 272:169–81. doi: 10.1016/j.jconrel.2018.01.001
22. Ferrara K, Pollard R, Borden MA. Ultrasound microbubble contrast agents: fundamentals and application to gene and drug delivery. *Annu Rev Biomed Eng*. (2007) 9:415–47. doi: 10.1146/annurev.bioeng.8.061505.095852
23. Kooiman K, Roovers S, Langeveld SAG, Kleven RT, Dewitte H, O'Reilly MA, et al. Ultrasound-responsive cavitation nuclei for therapy and drug delivery. *Ultrasound Med Biol*. (2020) 46:1296–325. doi: 10.1016/j.ultrasmedbio.2020.01.002
24. Carpentier A, Canney M, Vignot A, Reina V, Beccaria K, Horodyckid C, et al. Clinical trial of blood-brain barrier disruption by pulsed ultrasound. *Sci Transl Med*. (2016) 8:343re2. doi: 10.1126/scitranslmed.aaf6086
25. Lipsman N, Meng Y, Bethune AJ, Huang Y, Lam B, Masellis M, et al. Blood–brain barrier opening in Alzheimer's disease using MR-guided focused ultrasound. *Nat Commun*. (2018) 9:1–8. doi: 10.1038/s41467-018-04529-6
26. Mitchell MJ, Billingsley MM, Haley RM, Wechsler ME, Peppas NA, Langer R. Engineering precision nanoparticles for drug delivery. *Nat Rev Drug Discov*. (2020) 20:101–24. doi: 10.1038/s41573-020-0090-8
27. Maeda H, Wu J, Sawa T, Matsumura Y, Hori K. Tumor vascular permeability and the EPR effect in macromolecular therapeutics: a review. *J Control Release*. (2000) 65:271–84. doi: 10.1016/S0168-3659(99)00248-5
28. Pearce AK, O'Reilly RK. Insights into active targeting of nanoparticles in drug delivery: advances in clinical studies and design considerations for cancer nanomedicine. *Bioconjug Chem*. (2019) 30:2300–11. doi: 10.1021/acs.bioconjchem.9b00456
29. Pellow C, Goertz DE, Zheng G. Breaking free from vascular confinement: status and prospects for submicron ultrasound contrast agents. *Wiley Interdiscip Rev Nanomed Nanobiotechnol*. (2018) 10:e1502. doi: 10.1002/wnan.1502
30. Perera RH, Hernandez C, Zhou H, Kota P, Burke A, Exner AA. Ultrasound imaging beyond the vasculature with new generation contrast agents. *Wiley Interdiscip Rev NanomedNanobiotechnol*. (2015) 7:593–608. doi: 10.1002/wnan.1326
31. Ho YJ, Yeh CK. Concurrent anti-vascular therapy and chemotherapy in solid tumors using drug-loaded acoustic nanodroplet vaporization. *Acta Biomater*. (2017) 49:472–85. doi: 10.1016/j.actbio.2016.11.018
32. Seo M, Zhu S, Matsuura N. Diethyl ether as a drug-loading and sizereducing cosolvent to produce monodisperse, nanoscale perfluorocarbon agents. *IEEE Int Ultrason Symp*. (2015) 1–4. doi: 10.1109/ULTSYM.2015.0385
33. Sheeran PS, Luois S, Dayton PA, Matsunaga TO. Formulation and acoustic studies of a new phase-shift agent for diagnostic and therapeutic ultrasound. *Langmuir*. (2011) 27:10412–20. doi: 10.1021/la2013705
34. Shapiro MG, Goodwill PW, Neogy A, Yin M, Foster FS, Schaffer DV, et al. Biogenic gas nanostructures as ultrasonic molecular reporters. *Nat Nanotechnol*. (2014) 9:311–6. doi: 10.1038/nnano.2014.32
35. Cherin E, Melis JM, Bourdeau RW, Yin M, Kochmann DM, Foster FS, et al. Acoustic behavior of halobacterium salinarum gas vesicles in the high-frequency range: experiments and modeling. *Ultrasound Med Biol*. (2017) 43:1016–30. doi: 10.1016/j.ultrasmedbio.2016.12.020
36. Hitchcock KE, Caudell DN, Sutton JT, Klegerman ME, Vela D, Pyne-Geithman GJ, et al. Ultrasound-enhanced delivery of targeted echogenic liposomes in a novel ex vivo mouse aorta model. *J Control Release*. (2010) 144:288–95. doi: 10.1016/j.jconrel.2010.02.030
37. Kwan JJ, Myers R, Coviello CM, Graham SM, Shah AR, Stride E, et al. Ultrasound-propelled nanocups for drug delivery. *Small*. (2015) 11:5305–14. doi: 10.1002/smll.201501322
38. Kwan JJ, Borden MA. Lipid monolayer collapse and microbubble stability. *Adv Colloid Interface Sci*. (2012) 183–184:82–99. doi: 10.1016/j.cis.2012.08.005
39. Matsuura N, Koonar E, Zhu S, Leung B, Seo M, Sivapalan N, et al. Inducing antivascular effects in tumors with ultrasound stimulated micron-sized bubbles. *2015 IEEE Int Ultrason Symp IUS 2015*. (2015) 3–6. doi: 10.1109/ULTSYM.2015.0315
40. Ouyang B, Poon W, Zhang YN, Lin ZP, Kingston BR, Tavares AJ, et al. The dose threshold for nanoparticle tumour delivery. *Nat Mater*. (2020) 19:1362–71. doi: 10.1038/s41563-020-0755-z
41. de Leon A, Perera R, Nittayacharn P, Cooley M, Jung O, Exner AA. Ultrasound contrast agents and delivery systems in cancer detection and therapy. *Adv Cancer Res*. (2018) 139:57–84. doi: 10.1016/bs.acr.2018.04.002
42. Stride E, Segers T, Lajoinie G, Cherkaoui S, Bettinger T, Versluis M, et al. Microbubble agents: new directions. *Ultrasound Med Biol*. (2020) 46:1326–43. doi: 10.1016/j.ultrasmedbio.2020.01.027
43. Choi V, Rajora MA, Zheng G. Activating drugs with sound: mechanisms behind sonodynamic therapy and the role of nanomedicine. *Bioconjug Chem*. (2020) 31:967–89. doi: 10.1021/acs.bioconjchem.0c00029
44. Helfield B. A review of phospholipid encapsulated ultrasound contrast agent microbubble physics. *Ultrasound Med Biol*. (2019) 45:282–300. doi: 10.1016/j.ultrasmedbio.2018.09.020
45. Versluis M, Stride E, Lajoinie G, Dollet B, Segers T. Ultrasound contrast agent modeling: a review. *Ultrasound Med Biol*. (2020) 46:2117–44. doi: 10.1016/j.ultrasmedbio.2020.04.014
46. Perera RH, Wu H, Peiris P, Hernandez C, Burke A, Zhang H, et al. Improving performance of nanoscale ultrasound contrast agents using N,N-diethylacrylamide stabilization. *Nanomed Nanotechnol Biol Med*. (2017) 13:59–67. doi: 10.1016/j.nano.2016.08.020
47. Pellow C, Acconcia C, Zheng G, Goertz DE. Threshold-dependent nonlinear scattering from porphyrin nanobubbles for vascular and extravascular applications. *Phys Med Biol*. (2018) 63:215001. doi: 10.1088/1361-6560/aae571
48. Emmer M, van Wamel A, Goertz DE, de Jong N. The onset of microbubble vibration. *Ultrasound Med Biol*. (2007) 33:941–9. doi: 10.1016/j.ultrasmedbio.2006.11.004
49. Faez T, Emmer M, Docter M, Sijl J, Versluis M, de Jong N. Characterizing the subharmonic response of phospholipid-coated microbubbles for carotid imaging. *Ultrasound Med Biol*. (2011) 37:958–70. doi: 10.1016/j.ultrasmedbio.2011.02.017
50. Helfield BL, Goertz DE. Nonlinear resonance behavior and linear shell estimates for Definity™ and MicroMarker™ assessed with acoustic microbubble spectroscopy. *Cit J Acoust Soc Am*. (2013) 133:1158. doi: 10.1121/1.4774379
51. Eisenbrey JR, Dave JK, Forsberg F. Recent technological advancements in breast ultrasound. *Ultrasonics*. (2016) 70:183–90. doi: 10.1016/j.ultras.2016.04.021
52. Stuart Foster F, Hossack J, Lee Adamson S. Micro-ultrasound for preclinical imaging. *Interface Focus*. (2011) 1:576–601. doi: 10.1098/rsfs.2011.0037
53. Nissen SE, Yock P. Intravascular ultrasound: novel pathophysiological insights and current clinical applications. *Circulation*. (2001) 103:604–16. doi: 10.1161/01.CIR.103.4.604

54. Nicholls SJ, Murat Tuzcu E, Sipahi I, Schoenhagen P, Nissen SE. Intravascular ultrasound in cardiovascular medicine. *Circulation*. (2006) 114:e55–9. doi: 10.1161/CIRCULATIONAHA.106.637942
55. Moreno PR, Purushothaman KR, Fuster V, Echeverri D, Truszczynska H, Sharma SK, et al. Plaque neovascularization is increased in ruptured atherosclerotic lesions of human aorta: Implications for plaque vulnerability. *Circulation*. (2004) 110:2032–8. doi: 10.1161/01.CIR.0000143233.87854.23
56. McCarthy MJ, Loftus IM, Thompson MM, Jones L, London NJM, Bell PRF, et al. Angiogenesis and the atherosclerotic carotid plaque: an association between symptomatology and plaque morphology. *J Vasc Surg*. (1999) 30:261–8. doi: 10.1016/S0741-5214(99)70136-9
57. Hamilton AJ, Huang SL, Warnick D, Rabbat M, Kane B, Nagaraj A, et al. Intravascular ultrasound molecular imaging of atheroma components *in vivo*. *J Am Coll Cardiol*. (2004) 43:453–60. doi: 10.1016/j.jacc.2003.07.048
58. Gorce JM, Arditi M, Schneider M. Influence of bubble size distribution on the echogenicity of ultrasound contrast agents: a study of sonovue(TM). *Invest Radiol*. (2000) 35:661–71. doi: 10.1097/00004424-200011000-00003
59. Sontum PC. Physicochemical characteristics of Sonazoid^{TM}, a new contrast agent for ultrasound imaging. *Ultrasound Med Biol*. (2008) 34:824–33. doi: 10.1016/j.ultrasmedbio.2007.11.006
60. Chowdhury SM, Lee T, Willmann JK. Ultrasound-guided drug delivery in cancer. *Ultrasonography*. (2017) 36:171–84. doi: 10.14366/usg.17021
61. Chen HH, Matkar PN, Afrasiabi K, Kuliszewski MA, Leong-Poi H. Prospect of ultrasound-mediated gene delivery in cardiovascular applications. *Expert Opin Biol Ther*. (2016) 16:815–26. doi: 10.1517/14712598.2016.1169268
62. Inaba Y, Lindner JR. Molecular imaging of disease with targeted contrast ultrasound imaging. *Transl Res*. (2012) 159:140–8. doi: 10.1016/j.trsl.2011.12.001
63. Song KH, Fan AC, Hinkle JJ, Newman J, Borden MA, Harvey BK. Microbubble gas volume: a unifying dose parameter in blood-brain barrier opening by focused ultrasound. *Theranostics*. (2017) 7:144–52. doi: 10.7150/thno.15987
64. Zhang X, Wu M, Zhang Y, Zhang J, Su J, Yang C. Molecular imaging of atherosclerotic plaque with lipid nanobubbles as targeted ultrasound contrast agents. *Colloids Surf B Biointerfaces*. (2020) 189:110861. doi: 10.1016/j.colsurfb.2020.110861
65. Du J, Li XY, Hu H, Xu L, Yang SP, Li FH. Preparation and imaging investigation of dual-targeted C3F8-filled PLGA nanobubbles as a novel ultrasound contrast agent for breast cancer. *Sci Rep*. (2018) 8:1–18. doi: 10.1038/s41598-018-21502-x
66. Xie F, Li ZP, Wang HW, Fei X, Jiao ZY, Tang WB, et al. Evaluation of liver ischemia-reperfusion injury in rabbits using a nanoscale ultrasound contrast agent targeting ICAM-1. *PLoS ONE*. (2016) 11:1–21. doi: 10.1371/journal.pone.0153805
67. Gao Y, Hernandez C, Yuan HX, Lilly J, Kota P, Zhou H, et al. Ultrasound molecular imaging of ovarian cancer with CA-125 targeted nanobubble contrast agents. *Nanomed Nanotechnol Biol Med*. (2017) 13:2159–68. doi: 10.1016/j.nano.2017.06.001
68. Yang H, Cai W, Xu L, Lv X, Qiao Y, Li P, et al. Nanobubble-Affibody: novel ultrasound contrast agents for targeted molecular ultrasound imaging of tumor. *Biomaterials*. (2015) 37:279–88. doi: 10.1016/j.biomaterials.2014.10.013
69. Perera R, de Leon A, Wang X, Wang Y, Ramamurthy G, Peiris P, et al. Real time ultrasound molecular imaging of prostate cancer with PSMA-targeted nanobubbles. *Nanomed Nanotechnol Biol Med*. (2020) 28:102213. doi: 10.1016/j.nano.2020.102213
70. Yu Z, Hu M, Li Z, Dan Xu, Zhu L, Guo Y, et al. Anti-G250 nanobody-functionalized nanobubbles targeting renal cell carcinoma cells for ultrasound molecular imaging. *Nanotechnology*. (2020) 31:205101. doi: 10.1088/1361-6528/ab7040
71. Wu W, Zhang Z, Zhuo L, Zhou L, Liu P, He Y, et al. Ultrasound molecular imaging of acute cellular cardiac allograft rejection in rat with t-cell-specific nanobubbles. *Transplantation*. (2013) 96:543–9. doi: 10.1097/TP.0b013e31829b759f
72. Liu J, Chen Y, Wang G, Lv Q, Yang Y, Wang J, et al. Ultrasound molecular imaging of acute cardiac transplantation rejection using nanobubbles targeted to T lymphocytes. *Biomaterials*. (2018) 162:200–7. doi: 10.1016/j.biomaterials.2018.02.017
73. Jain RK. Determinants of tumor blood flow: a review. *Cancer Res*. (1988) 48:2641–58.
74. Marmottant P, Hilgenfeldt S. Controlled vesicle deformation and lysis by single oscillating bubbles. *Nature*. (2003) 423:153–6. doi: 10.1038/nature01613
75. Chen H, Brayman AA, Kreider W, Bailey MR, Matula TJ. Observations of translation and jetting of ultrasound-activated microbubbles in mesenteric microvessels. *Ultrasound Med Biol*. (2011) 37:2139–48. doi: 10.1016/j.ultrasmedbio.2011.09.013
76. Lentacker I, De Smedt SC, Sanders NN. Drug loaded microbubble design for ultrasound triggered delivery. *Soft Matter*. (2009) 5:2161–70. doi: 10.1039/b823051j
77. Ma L, Wang Y, Zhang S, Qian X, Xue N, Jiang Z, et al. Deep penetration of targeted nanobubbles enhanced cavitation effect on thrombolytic capacity. *Bioconjug Chem*. (2020) 31:369–74. doi: 10.1021/acs.bioconjchem.9b00653
78. Ramirez DG, Abenojar E, Hernandez C, Lorberbaum DS, Papazian LA, Passman S, et al. Contrast-enhanced ultrasound with sub-micron sized contrast agents detects insulitis in mouse models of type1 diabetes. *Nat Commun*. (2020) 11:1–13. doi: 10.1038/s41467-020-15957-8
79. Shang M, Wang K, Guo L, Duan S, Lu Z, Li J. Development of novel ST68/PLA-PEG stabilized ultrasound nanobubbles for potential tumor imaging and theranostic. *Ultrasonics*. (2019) 99:105947. doi: 10.1016/j.ultras.2019.105947
80. Gao S, Cheng X, Li J. Lipid nanobubbles as an ultrasound-triggered artesunate delivery system for imaging-guided, tumor-targeted chemotherapy. *Onco Targets Ther*. (2019) 12:1841–50. doi: 10.2147/OTT.S190208
81. Nguyen AT, Wrenn SP. Acoustically active liposome-nanobubble complexes for enhanced ultrasonic imaging and ultrasound-triggered drug delivery. *Wiley Interdiscip Rev Nanomed Nanobiotechnol*. (2014) 6:316–25. doi: 10.1002/wnan.1255
82. Jiang Q, Hao S, Xiao X, Yao J, Ou B, Zhao Z, et al. Production and characterization of a novel long-acting Herceptin-targeted nanobubble contrast agent specific for Her-2-positive breast cancers. *Breast Cancer*. (2016) 23:445–55. doi: 10.1007/s12282-014-0581-8
83. Xing Z, Wang J, Ke H, Zhao B, Yue X, Dai Z, et al. The fabrication of novel nanobubble ultrasound contrast agent for potential tumor imaging. *Nanotechnology*. (2010) 21:145607. doi: 10.1088/0957-4484/21/14/145607
84. Wang Y, Li X, Zhou Y, Huang P, Xu Y. Preparation of nanobubbles for ultrasound imaging and intracelluar drug delivery. *Int J Pharm*. (2010) 384:148–53. doi: 10.1016/j.ijpharm.2009.09.027
85. Zhang J, Chen Y, Deng C, Zhang L, Sun Z, Wang J, et al. The optimized fabrication of a novel nanobubble for tumor imaging. *Front Pharmacol*. (2019) 10:1–15. doi: 10.3389/fphar.2019.00610
86. Upadhyay A, Dalvi S. Microbubble formulations: synthesis, stability, modeling and biomedical applications. *Ultrasound Med Biol*. (2019) 45:1–5. doi: 10.1016/j.ultrasmedbio.2018.09.022
87. Goertz DE, de Jong N, van der Steen AFW. Attenuation and size distribution measurements of definity^{TM} and manipulated definity^{TM} populations. *Ultrasound Med Biol*. (2007) 33:1376–88. doi: 10.1016/j.ultrasmedbio.2007.03.009
88. Feshitan JA, Chen CC, Kwan JJ, Borden MA. Microbubble size isolation by differential centrifugation. *J Colloid Interface Sci*. (2009) 329:316–24. doi: 10.1016/j.jcis.2008.09.066
89. Helfield BL, Cherin E, Foster FS, Goertz DE. Investigating the subharmonic response of individual phospholipid encapsulated microbubbles at high frequencies: a comparative study of five agents. *Ultrasound Med Biol*. (2012) 38:846–63. doi: 10.1016/j.ultrasmedbio.2012.01.011
90. Peyman SA, McLaughlan JR, Abou-Saleh RH, Marston G, Johnson BRG, Freear S, et al. On-chip preparation of nanoscale contrast agents towards high-resolution ultrasound imaging. *Lab Chip*. (2016) 16:679–87. doi: 10.1039/C5LC01394A
91. Blum NT, Yildirim A, Chattaraj R, Goodwin AP. Nanoparticles formed by acoustic destruction of microbubbles and their utilization for imaging and effects on therapy by high intensity focused ultrasound. *Theranostics*. (2017) 7:694–702. doi: 10.7150/thno.17522

92. Borden MA, Pu G, Runner GJ, Longo ML. Surface phase behavior and microstructure of lipid/PEG-emulsifier monolayer-coated microbubbles. *Colloids Surf B Biointerfaces*. (2004) 35:209–23. doi: 10.1016/j.colsurfb.2004.03.007
93. Kato T, Nishimiya M, Kawata A, Kishida K, Suzuri K, Saito M, et al. Quantitative 31P NMR method for individual and concomitant determination of phospholipid classes in polar lipid samples. *J Oleo Sci*. (2018) 67:1279–89. doi: 10.5650/jos.ess18062
94. Helfield BL, Huo X, Williams R, Goertz DE. The effect of preactivation vial temperature on the acoustic properties of definity™. *Ultrasound Med Biol*. (2012) 38:1298–305. doi: 10.1016/j.ultrasmedbio.2012.03.005
95. de Jong N, Emmer M, Chin CT, Bouakaz A, Mastik F, Lohse D, et al. "Compression-only" behavior of phospholipid-coated contrast bubbles. *Ultrasound Med Biol*. (2007) 33:653–6. doi: 10.1016/j.ultrasmedbio.2006.09.016
96. van der Meer S, Dollet B, Chin CT, Bouakaz A, Voormolen M, de Jong N, et al. Microbubble spectroscopy of ultrasound contrast agents. *J Acoust Soc Am*. (2007) 120:3327. doi: 10.1121/1.4781240
97. Pellow C, Tan J, Chérin E, Demore CEM, Zheng G, Goertz DE. High frequency ultrasound nonlinear scattering from porphyrin nanobubbles. *Ultrasonics*. (2021) 110:106245. doi: 10.1016/j.ultras.2020.106245
98. Mai L, Yao A, Li J, Wei Q, Yuchi M, He X, et al. Cyanine 5.5 conjugated nanobubbles as a tumor selective contrast agent for dual ultrasound-fluorescence imaging in a mouse model. *PLoS ONE*. (2013) 8:1–10. doi: 10.1371/journal.pone.0061224
99. Cai W Bin, Yang HL, Zhang J, Yin JK, Yang YL, Yuan LJ, et al. The optimized fabrication of nanobubbles as ultrasound contrast agents for tumor imaging. *Sci Rep*. (2015) 5:1–11. doi: 10.1038/srep13725
100. Wheatley MA, Forsberg F, Dube N, Patel M, Oeffinger BE. Surfactant-stabilized contrast agent on the nanoscale for diagnostic ultrasound imaging. *Ultrasound Med Biol*. (2006) 32:83–93. doi: 10.1016/j.ultrasmedbio.2005.08.009
101. Hernandez C, Abenojar EC, Hadley J, De Leon AC, Coyne R, Perera R, et al. Sink or float? Characterization of shell-stabilized bulk nanobubbles using a resonant mass measurement technique. *Nanoscale*. (2019) 11:851–5. doi: 10.1039/C8NR08763F
102. Wu B, Qiao Q, Han X, Jing H, Zhang H, Liang H, et al. Targeted nanobubbles in low-frequency ultrasound-mediated gene transfection and growth inhibition of hepatocellular carcinoma cells. *Tumor Biol*. (2016) 37:12113–21. doi: 10.1007/s13277-016-5082-2
103. Yin T, Wang P, Zheng R, Zheng B, Cheng D, Zhang X, et al. IJN-28830-nanobubbles-for-enhanced-ultrasound-imaging-of-tumors. *Int J Nanomedicine*. (2012) 7:895–904. doi: 10.2147/IJN.S28830
104. Pellow C, Cherin E, Abenojar EC, Exner AA, Zheng G, Demore CEM, et al. High frequency array-based nanobubble nonlinear imaging in a phantom and in vivo. *IEEE Trans Ultrason Ferroelectr Freq Control*. (2021) 1-15. doi: 10.1109/TUFFC.2021.3055141
105. Pellow C, O'Reilly MA, Hynynen K, Zheng G, Goertz DE. Simultaneous intravital optical and acoustic monitoring of ultrasound-triggered nanobubble generation and extravasation. *Nano Lett*. (2020) 20:4512–9. doi: 10.1021/acs.nanolett.0c01310
106. Pellow C, Abenojar EC, Exner AA, Zheng G, Goertz DE. Concurrent visual and acoustic tracking of passive and active delivery of nanobubbles to tumors. *Theranostics*. (2020) 10:11690–706. doi: 10.7150/thno.51316
107. De Leon A, Perera R, Hernandez C, Cooley M, Jung O, Jeganathan S, et al. Contrast enhanced ultrasound imaging by nature-inspired ultrastable echogenic nanobubbles. *Nanoscale*. (2019) 11:15647–58. doi: 10.1039/C9NR04828F
108. Becher H, Burns PN. *Handbook of Contrast Echocardiography*. New York, NY: Springer (2000).
109. Talu E, Powell RL, Longo ML, Dayton PA. Needle size and injection rate impact microbubble contrast agent population. *Ultrasound Med Biol*. (2008) 34:1182–5. doi: 10.1016/j.ultrasmedbio.2007.12.018
110. Browning RJ, Mulvana H, Tang M, Hajnal JV, Wells DJ, Eckersley RJ. Influence of needle gauge on in vivo ultrasound and microbubble-mediated gene transfection. *Ultrasound Med Biol*. (2011) 37:1531–7. doi: 10.1016/j.ultrasmedbio.2011.05.019
111. Mullin L, Gessner R, Kwan J, Kaya M, Borden MA, Dayton PA. Effect of anesthesia carrier gas on in vivo circulation times of ultrasound microbubble contrast agents in rats. *Contrast Media Mol Imaging*. (2011) 6:126–31. doi: 10.1002/cmmi.414
112. Mulvana H, Stride E, Hajnal JV, Eckersley RJ. Temperature dependent behavior of ultrasound contrast agents. *Ultrasound Med Biol*. (2010) 36:925–34. doi: 10.1016/j.ultrasmedbio.2010.03.003
113. Lantheus Medical Imaging Inc. Definity® (Perflutren Lipid Microsphere) Injectable Suspension [package insert]. *US Food Drug Adm*. (2001) 1–18. Available online at: https://www.definityimaging.com/pdf/DEFINITY%20Marketing%20PI%205159870820.pdf
114. Stride E, Saffari N. Investigating the significance of multiple scattering in ultrasound contrast agent particle populations. *IEEE Trans Ultrason Ferroelectr Freq Control*. (2005) 52:2332–45. doi: 10.1109/TUFFC.2005.1563278
115. Postema M, Marmottant P, Lancée CT, Hilgenfeldt S, Jong N De. Ultrasound-induced microbubble coalescence. *Ultrasound Med Biol*. (2004) 30:1337–44. doi: 10.1016/j.ultrasmedbio.2004.08.008
116. Tanter M, Fink M. Ultrafast imaging in biomedical ultrasound. *IEEE Trans Ultrason Ferroelectr Freq Control*. (2014) 61:102–19. doi: 10.1109/TUFFC.2014.6689779
117. Sigrist RMS, Liau J, Kaffas A El, Chammas MC, Willmann JK. Ultrasound elastography: review of techniques and clinical applications. *Theranostics*. (2017) 7:1303–29. doi: 10.7150/thno.18650
118. Villemain O, Baranger J, Friedberg MK, Papadacci C, Dizeux A, Messas E, et al. Ultrafast ultrasound imaging in pediatric and adult cardiology: techniques, applications, and perspectives. *JACC Cardiovasc Imaging*. (2020) 13:1771–91. doi: 10.1016/j.jcmg.2019.09.019
119. Demené C, Mairesse J, Baranger J, Tanter M, Baud O. Ultrafast Doppler for neonatal brain imaging. *Neuroimage*. (2019) 185:851–6. doi: 10.1016/j.neuroimage.2018.04.016
120. Couture O, Hingot V, Heiles B, Muleki-Seya P, Tanter M. Ultrasound localization microscopy and super-resolution: a state of the art. *IEEE Trans Ultrason Ferroelectr Freq Control*. (2018) 65:1304–20. doi: 10.1109/TUFFC.2018.2850811
121. Lin F, Shelton SE, Espíndola D, Rojas JD, Pinton G, Dayton PA. 3-D ultrasound localization microscopy for identifying microvascular morphology features of tumor angiogenesis at a resolution beyond the diffraction limit of conventional ultrasound. *Theranostics*. (2017) 7:196–204. doi: 10.7150/thno.16899
122. O'Reilly MA, Hynynen K. A super-resolution ultrasound method for brain vascular mapping. *Med Phys*. (2013) 40:1–7. doi: 10.1118/1.4823762
123. Blackmore J, Shrivastava S, Sallet J, Butler CR, Cleveland RO. Ultrasound neuromodulation: a review of results, mechanisms and safety. *Ultrasound Med Biol*. (2019) 45:1509–36. doi: 10.1016/j.ultrasmedbio.2018.12.015
124. Burgess A, Shah K, Hough O, Hynynen K. Focused ultrasound-mediated drug delivery through the blood–brain barrier. *Expert Rev Neurother*. (2015) 15:477–91. doi: 10.1586/14737175.2015.1028369
125. Lea-Banks H, Meng Y, Wu SK, Belhadjhamida R, Hamani C, Hynynen K. Ultrasound-sensitive nanodroplets achieve targeted neuromodulation. *J Control Release*. (2021) 332:30–9. doi: 10.1016/j.jconrel.2021.02.010
126. Lea-Banks H, O'Reilly MA, Hamani C, Hynynen K. Localized anesthesia of a specific brain region using ultrasound-responsive barbiturate nanodroplets. *Theranostics*. (2020) 10:2849–58. doi: 10.7150/thno.41566
127. Ho YJ, Li JP, Fan CH, Liu HL, Yeh CK. Ultrasound in tumor immunotherapy: current status and future developments. *J Control Release*. (2020) 323:12–23. doi: 10.1016/j.jconrel.2020.04.023
128. Unga J, Hashida M. Ultrasound induced cancer immunotherapy. *Adv Drug Deliv Rev*. (2014) 72:144–53. doi: 10.1016/j.addr.2014.03.004
129. Bulner S, Prodeus A, Gariepy J, Hynynen K, Goertz DE. Enhancing checkpoint inhibitor therapy with ultrasound stimulated microbubbles. *Ultrasound Med Biol*. (2019) 45:500–12. doi: 10.1016/j.ultrasmedbio.2018.10.002
130. Alkins R, Burgess A, Kerbel R, Wels WS, Hynynen K. Early treatment of HER2-amplified brain tumors with targeted NK-92 cells and focused ultrasound improves survival. *Neuro Oncol*. (2016) 18:974–81. doi: 10.1093/neuonc/nov318

131. Zolochevska O, Xia X, Williams BJ, Ramsay A, Li S, Figueiredo ML. Sonoporation delivery of interleukin-27 gene therapy efficiently reduces prostate tumor cell growth in vivo. *Hum Gene Ther*. (2011) 22:1537–50. doi: 10.1089/hum.2011.076
132. Huynh E, Leung BYC, Helfield BL, Shakiba M, Gandier JA, Jin CS, et al. In situ conversion of porphyrin microbubbles to nanoparticles for multimodality imaging. *Nat Nanotechnol*. (2015) 10:325–32. doi: 10.1038/nnano.2015.25
133. Fielding D, Kurimoto N. Endobronchial ultrasound-guided transbronchial needle aspiration for diagnosis and staging of lung cancer. *Clin Chest Med*. (2018) 39:111–23. doi: 10.1016/j.ccm.2017.11.012
134. Izadifar Z, Izadifar Z, Chapman D, Babyn P. An introduction to high intensity focused ultrasound: systematic review on principles, devices, and clinical applications. *J Clin Med*. (2020) 9:460. doi: 10.3390/jcm9020460
135. ter Haar G, Coussios C. High intensity focused ultrasound: physical principles and devices. *Int J Hyperth*. (2007) 23:89–104. doi: 10.1080/02656730601186138
136. Chaussy CG, Thüroff S. High-intensity focused ultrasound for the treatment of prostate cancer: a review. *J Endourol*. (2017) 31:S30–7. doi: 10.1089/end.2016.0548
137. Bessiere F, N'djin WA, Colas EC, Chavrier F, Greillier P, Chapelon JY, et al. Ultrasound-guided transesophageal high-intensity focused ultrasound cardiac ablation in a beating heart: a pilot feasibility study in pigs. *Ultrasound Med Biol*. (2016) 42:1848–61. doi: 10.1016/j.ultrasmedbio.2016.03.007
138. Yu H, Chen S, Cao P. Synergistic bactericidal effects and mechanisms of low intensity ultrasound and antibiotics against bacteria: a review. *Ultrason Sonochem*. (2011) 19:377–82. doi: 10.1016/j.ultsonch.2011.11.010
139. Horsley H, Owen J, Browning R, Carugo D, Malone-Lee J, Stride E, et al. Ultrasound-activated microbubbles as a novel intracellular drug delivery system for urinary tract infection. *J Control Release*. (2019) 301:166–75. doi: 10.1016/j.jconrel.2019.03.017
140. Czarnota GJ, Karshafian R, Burns PN, Wong S, Al Mahrouki A, Lee JW, et al. Tumor radiation response enhancement by acoustical stimulation of the vasculature. *Proc Natl Acad Sci U S A*. (2012) 109:E2033–41. doi: 10.1073/pnas.1200053109
141. Forbrich A, Paproski R, Hitt M, Zemp R. Microbubble-enhanced ultrasound liberation of mrna biomarkers in vitro. *Ultrasound Med Biol*. (2013) 39:1087–93. doi: 10.1016/j.ultrasmedbio.2012.12.015
142. Zhu L, Cheng G, Ye D, Nazeri A, Yue Y, Liu W, et al. Focused ultrasound-enabled brain tumor liquid biopsy. *Sci Rep*. (2018) 8:1–9. doi: 10.1038/s41598-018-24516-7
143. Perera RH, Solorio L, Wu H, Gangolli M, Silverman E, Hernandez C,et al. Nanobubble ultrasound contrast agents for enhanced delivery of thermal sensitizer to tumors undergoing radiofrequency ablation. *Pharm Res*. (2014) 31:1407–17. doi: 10.1007/s11095-013-1100-x
144. Xiang Y, Bernards N, Hoang B, Zheng J, Matsuura N. Perfluorocarbon nanodroplets can reoxygenate hypoxic tumors in vivo without carbogen breathing. *Nanotheranostics*. (2019) 3:135–44. doi: 10.7150/ntno.29908

Conflict of Interest: The authors declare that the research was conducted in the absence of any commercial or financial relationships that could be construed as a potential conflict of interest.